Psychophysical Reverse Correlation Revealed Broader Orientation Tuning and Prolonged Reaction Time in Amblyopia

Jinli Zhu,[1] Xiaowei Ruan,[1] Cheng Li,[1] Junli Yuan,[1] Yan Yang,[1] Wenhua Zhang,[1] Hanyi Zhang,[1] Zuopao Zhuo,[1] Fang-Fang Yan,[2,3] Chang-Bing Huang,[2,3] and Fang Hou[1]

[1]School of Ophthalmology & Optometry and Eye Hospital, Wenzhou Medical University, Wenzhou, Zhejiang, China
[2]Key Laboratory of Behavioral Science, Institute of Psychology, Chinese Academy of Sciences, Chaoyang District, Beijing, China
[3]Department of Psychology, University of Chinese Academy of Sciences, Shijingshan District, Beijing, China

Correspondence: Chang-Bing Huang, Key Laboratory of Behavioral Science, Institute of Psychology, Chinese Academy of Sciences, 16 Lincui Road, Chaoyang District, Beijing 100101, China; huangcb@psych.ac.cn.
Fang Hou, School of Ophthalmology & Optometry and Eye Hospital, Wenzhou Medical University, 270 Xuanyuan Xi Road, Wenxhou, Zhejiang 325027, China; houf@eye.ac.cn.

Received: October 14, 2021
Accepted: April 18, 2022
Published: May 3, 2022

Citation: Zhu J, Ruan X, Li C, et al. Psychophysical reverse correlation revealed broader orientation tuning and prolonged reaction time in amblyopia. *Invest Ophthalmol Vis Sci.* 2022;63(5):3. https://doi.org/10.1167/iovs.63.5.3

Purpose. Neural selectivity of orientation is a fundamental property of visual system. We aim to investigate whether and how the orientation selectivity changes in amblyopia.

Methods. Seventeen patients with amblyopia (27.1 ± 7.1 years) and 18 healthy participants (25.1 ± 2.7 years) took part in this study. They were asked to continuously detect vertical gratings embedded in a stream of randomly oriented gratings. Using a technique of subspace reverse correlation, the orientation-time perceptive field (PF) for the atypical grating detection task was derived for each participant. Detailed comparisons were made between the PFs measured with the amblyopic and healthy eyes.

Results. The PF of the amblyopic eyes showed significant differences in orientation and time domain compared with that of the normal eyes (cluster-based permutation test, *p*s < 0.05), with broader bandwidth of orientation tuning (31.41 ± 10.59 degrees [mean ± SD] vs. 24.76 ± 6.85 degrees, $P = 0.039$) and delayed temporal dynamics (483 ± 68 ms vs. 425 ± 58 ms, $P = 0.015$). None of the altered PF properties correlated with the contrast sensitivity at 1 cycle per degree (c/deg) in amblyopia. No difference in PFs between the dominant and non-dominant eyes in the healthy group was found.

Conclusions. The altered orientation-time PF to the low spatial frequency and high contrast stimuli suggests amblyopes had coarser orientation selectivity and prolonged reaction time. The broader orientation tuning probably reflects the abnormal lateral interaction in the primary visual cortex, whereas the temporal delay might indicate a high level deficit.

Keywords: orientation, amblyopia, perceptive field, reverse correlation, lateral interaction

Amblyopia, also called lazy eye, is clinically characterized by reduced best-corrected visual acuity without detectable structural or pathological abnormalities.[1–5] It causes not only reduced visual acuity,[3–5] but also a variety of deficits in spatial vision, including deterioration of spatial contrast sensitivity,[6–10] stereoscopic vision,[11,12] and contour integration.[13,14] Aside from refractive error, it is the most frequent cause of vision loss in infants and children.[2]

Amblyopia is not only clinically important but also theoretically intriguing. It is believed to be a visual developmental disease where the abnormal visual experience caused by monocular strabismus, anisometropia, high refractive error, and/or form deprivation[15–17] disrupted the development of cortical functions during a sensitive period in visual development.[18–20] Amblyopia has been intensively studied in vision science because it reflects the neural consequences that occur when visual development is disrupted and can provide insights for understanding normal visual processing.

Neural selectivity of orientation is a fundamental property of the visual system,[21–24] and is commonly believed to emerge in the primary visual cortex.[25–29] The neural mechanism that determines the sharpness of the orientation tuning has received lots of attention, because the sharpness of tuning cannot be accounted by the thalamocortical feedforward connections[22,24,30,31] and must involve intracortical lateral interactions.[26,32–35] However, whether and how the sharpness of tuning is affected in amblyopia is still on debate.

The result from single cell recording suggested that amblyopia induced by nonselective visual blur or eye misalignment did not change the bandwidth of the orientation tuning of the V1 neurons in the cat[36–38] or in the macaque monkey.[39,40] On the other hand, the result from human studies showed that amblyopes exhibited impaired performance in orientation discrimination tasks. For example, patients with amblyopia had greater angular thresholds in discriminating the orientation of a narrowband

Copyright 2022 The Authors

This work is licensed under a Creative Commons Attribution-NonCommercial-NoDerivatives 4.0 International License.

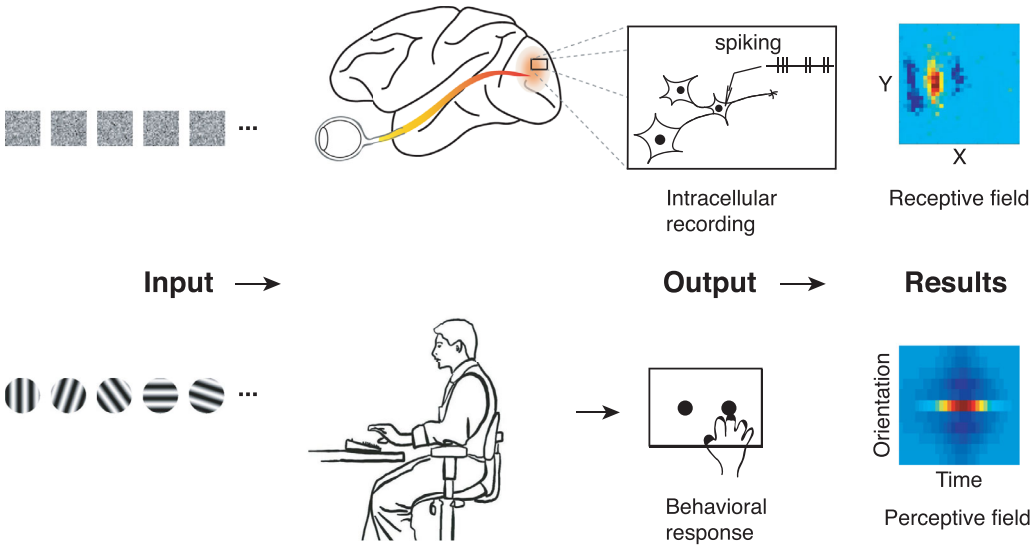

Figure 1. *Top row*: Reverse correlation in a typical electrophysiological experiment. The white noise images were presented to the animal and the neural spikes were recorded. Via reverse correlation, one can derive the receptive field of a particular neuron. *Bottom row*: Psychophysical reverse correlation in our experiment. Using reverse correlation, one can derive the weighting function of the visual system in the orientation-time domain for the task.

grating,[41,42] of the central grating with a surrounding background grating presented,[43] as well as of arrays consisting of randomly positioned Gabors.[44] As orientation discrimination involves decoding the population responses of a bank of orientation selective neurons, the increased orientation threshold could have reflected a broader tuning width in patients with amblyopia. Thus, it is difficult to exclude the potential contribution of the sensitivity loss to the abnormal orientation discrimination threshold.[39,45,46] With a different approach, Levi, Waugh, and Beard[47] measured the contrast threshold elevation of line detection as a function of mask orientation at the optimal spatial frequency in amblyopia. The orientation tuning estimated in the amblyopic eyes was found to be qualitatively similar in some participants but broader in others compared to the control eyes. No definitive conclusion was made.

Therefore, we attempt to directly probe the orientation tuning properties in both healthy and amblyopic participants with a paradigm of subspace reverse correlation.[26,48–50] By quantifying how random fluctuations of sensory stimuli influence human behavior, the psychophysical reverse correlation estimates how visual system weights the stimuli to guide behaviors[48,50,51] (Fig. 1; see Materials and Methods section for more details). The result of the psychophysical reverse correlation, termed as perceptive field (PF), is the psychophysical analogue of a neuronal receptive field, which depicts the weighting function of the visual system. The PF can provide insights that help understand how the visual system processes visual features.[51–53] By restricting the stimulus fluctuation in the orientation and time domains, we can derive the orientation-time PF of the observer for the task.

In the experiment, we asked participants with amblyopia to watch a randomly orientated grating sequence and, at the same time, to make the response as fast as possible whenever s/he saw a vertical grating. The responses were recorded and used to construct the PF for each participant. By comparing the PFs from amblyopic and normal observers, we hope to answer whether and how the property of orientation tuning is altered in amblyopia.

Materials and Methods

Participants

Seventeen participants with amblyopia (A1–A17, 27.1 ± 7.1 years, 8 men) and 18 control participants (N1–N18, 25.1 ± 2.7 years, 4 men) took part in the experiments. All participants with amblyopia had been previously diagnosed. At the time of the experiment, all participants had gone through detailed ophthalmologic and optometric examinations performed by the authors (J.Z., C.L., and Y.Y.). All participants, except A2, had astigmatism no more than 1.5 diopters (D), and showed no sign of any pathological abnormality. Participant A2 had congenital cataract and intraocular lens implantation in both eyes. A8 and A15 who had strabismus had surgically corrected the eye alignment. All of the control participants had normal or corrected-to-normal vision (logMAR $\leq$ 0.0). The contrast sensitivity functions (CSF) of the amblyopes (except A8 and A14) were measured using a Bayesian adaptive procedure, the description of which can be found elsewhere.[54] There was one participant in the control group and 11 participants in the amblyopic group who had experiences of psychophysical experiments. See the detailed information of the amblyopic participants in Table A1, Appendix A.

All participants were naive to the purpose of the study. They wore the best optical corrections at the test distance during the experiments. Eye dominance was determined with the hole-in-card method for each healthy subject.[55] The study adhered to the tenets of the Declaration of Helsinki and was approved by the institutional review board of human subject research of the Eye Hospital, Wenzhou Medical University. Written informed consent was obtained from each subject before the experiment.

Investigative Ophthalmology & Visual Science

Apparatus

The stimuli were generated using customized program written in MATLAB (The MathWorks Corp., Natick, MA, USA) with Psychtoolbox extension.[56] The program was run on an Intel NUC computer (Model: NUC6i7kYK; Intel Corporation, Santa Clara, CA, USA). The stimuli were displayed on a gamma-corrected monitor (ASUS SWIFT PG278QR; Asustek Computer Inc., Taipei, Taiwan). The monitor has been carefully tuned and calibrated so that the typical artifacts associated with liquid crystal displays (LCDs)[57,58] were minimalized and had negligible effects on participants' behavior. The display had a spatial resolution of 2560 × 1440 pixels and a refresh rate of 120 Hz. Each pixel subtended 0.009 degrees at a viewing distance of 1.44 m. The mean luminance was 100.7 cd/m^2. The key-pressing responses of subjects were recorded by an RT Box with the temporal resolution less than 26 µs[59] that ensured precise collection of response time. A chin/forehead rest was used to minimize head movement during the experiment. Observers viewed the stimuli monocularly with their best correction, if any, in a dark room. The eye not being tested was occluded by an opaque patch.

Stimuli

The stimulus used for measuring orientation tuning was a sequence of sinusoidal gratings presented at 30 Hz (each grating lasted 33.3 ms). The spatial frequency of the gratings was fixed at 1 cycle per degree (c/deg) and the contrast was 99%. The low spatial frequency and high contrast were used to compensate the sensitivity loss in amblyopia.[5,39,45,46] We chose 30 Hz presentation rate because it has been widely validated in previous researches[48,50] and the orientation tuning did not depend on temporal frequency.[60] The gratings had a circular aperture of 3.0-degree diameter and were presented at the center of the display. The orientation of each grating was chosen randomly from 0, 18, 36, 54, 72, 90, 108, 126, 144, and 162 degrees. The phase of the gratings was chosen from 0, $\pi/2$, π, and $3\pi/2$ randomly. The entire grating sequence consisted of 1800 gratings and lasted 60 seconds. The presentation order of the gratings with different orientations and phases was generated such that each orientation and phase combination was displayed for equal (45) times.

Procedure

Each trial started with the presentation of a black fixation dot (diameter of 0.28 degrees) at the center of the screen. The stimulus presentation began after the participant pressed the "SPACE" key. There was a brief tone signaling the onset of the grating sequence. The participants were asked to monitor the gratings presented at the center of the display and to press the button on the RT Box as fast as possible, whenever they noticed a vertical grating (90 degrees orientation). The time stamp of each key press was recorded. After the 60-second stimulus presentation, the fixation spot displayed again at the center of the screen. There was a total of 30 trials in a test session which lasted 45 minutes. No feedback was provided. The participants could take breaks between trials and press the "SPACE" key to initiate the stimulus presentation of the next trial.

The dominant eyes of the healthy participants and the amblyopic eyes of the participants with amblyopia were tested. All the participants were given practice trials to make sure they fully understood the task before formal experiment. To rule out the potential bias due to our choice of dominant eyes as the control, we additionally tested the nondominant eye of the eight (of 18) healthy participants who were able to revisit our laboratory. The CSFs of both eyes of the eight participants were also measured during the revisit.

Analysis

The PF for the orientation identification task was derived using a technique of subspace reverse correlation in the orientation-time domain.[26,48–50] The data were analyzed to reflect how the history of gratings in different orientations determined the button presses (Fig. 2a). Specifically, we looked at the grating orientations within 1 second periods (30 gratings) prior to each response (key press). The orientation histogram h(θ) was calculated for each time offset τ ($-30 \le \tau \le -1$, in the unit of stimulus frames). The results were averaged across the four phases. By dividing the total number of responses, we obtained the response probability p(θ) of a particular orientation θ at time τ (Fig. 2b). By concatenating p(θ) across all τs, we have the orientation-time PF(θ, τ), which had 330 data points in total, with 11 orientations (the response at orientation of 0 degrees was also been treated as that at orientation of 180 degrees) by 30 temporal delays (Figs. 2b, 2c).

To remove the temporal noise, the raw PF was convolved with a Gaussian window in the time domain to remove the frequency component greater than 10 Hz. To better extract the properties of the PF, a parametric model[26] was fitted to the temporally smoothed PF data:

$$\mathrm{PF}(\theta,\tau) = \alpha(\tau)E(\theta) + \beta(\tau)I(\theta) + \gamma(\tau) + c, \quad (1)$$

where $E(\theta)$ and $I(\theta)$ were the excitation and inhibition component of the orientation tuning curve, respectively; $\alpha(\tau)$ and $\beta(\tau)$ controls how the excitation, inhibition tuning components evolve over time, respectively; whereas $\gamma(\tau)$ represented a non-orientation selective global component that evolves in time; whereas c represented the baseline guessing rate of the observer.

Both $E(\theta)$ and $I(\theta)$ are described by transformed von Mises distribution[26,61]:

$$E(\theta) = \frac{\exp(\kappa_E \cos(2(\theta-\theta_E))) - \exp(-\kappa_E)}{\exp(\kappa_E) - \exp(-\kappa_E)}, \quad (2a)$$

$$I(\theta) = \frac{\exp(\kappa_I \cos(2(\theta-\theta_I))) - \exp(-\kappa_I)}{\exp(\kappa_I) - \exp(-\kappa_I)}, \quad (2b)$$

where κ_E and κ_I determine the width of the excitation and inhibition tunings, respectively; and θ_E and θ_I represent the centers of the two components, separately. Given that the target was vertical grating for every participant, θ_E and θ_I were set to 90 degrees for simplicity in our analysis.

The temporal dynamics $\alpha(\tau)$, $\beta(\tau)$, and $\gamma(\tau)$ were described by three skewed Gaussian distributions.[26,62]

$$\alpha(\tau) = 2\, a_0 \phi\left(\frac{\tau-\tau_E}{\sigma_E}\right)\Phi\left(\eta_E\left(\frac{\tau-\tau_E}{\sigma_E}\right)\right), \quad (3a)$$

$$\beta(\tau) = 2\, \beta_0 \phi\left(\frac{\tau-\tau_I}{\sigma_I}\right)\Phi\left(\eta_I\left(\frac{\tau-\tau_I}{\sigma_I}\right)\right), \quad (3b)$$

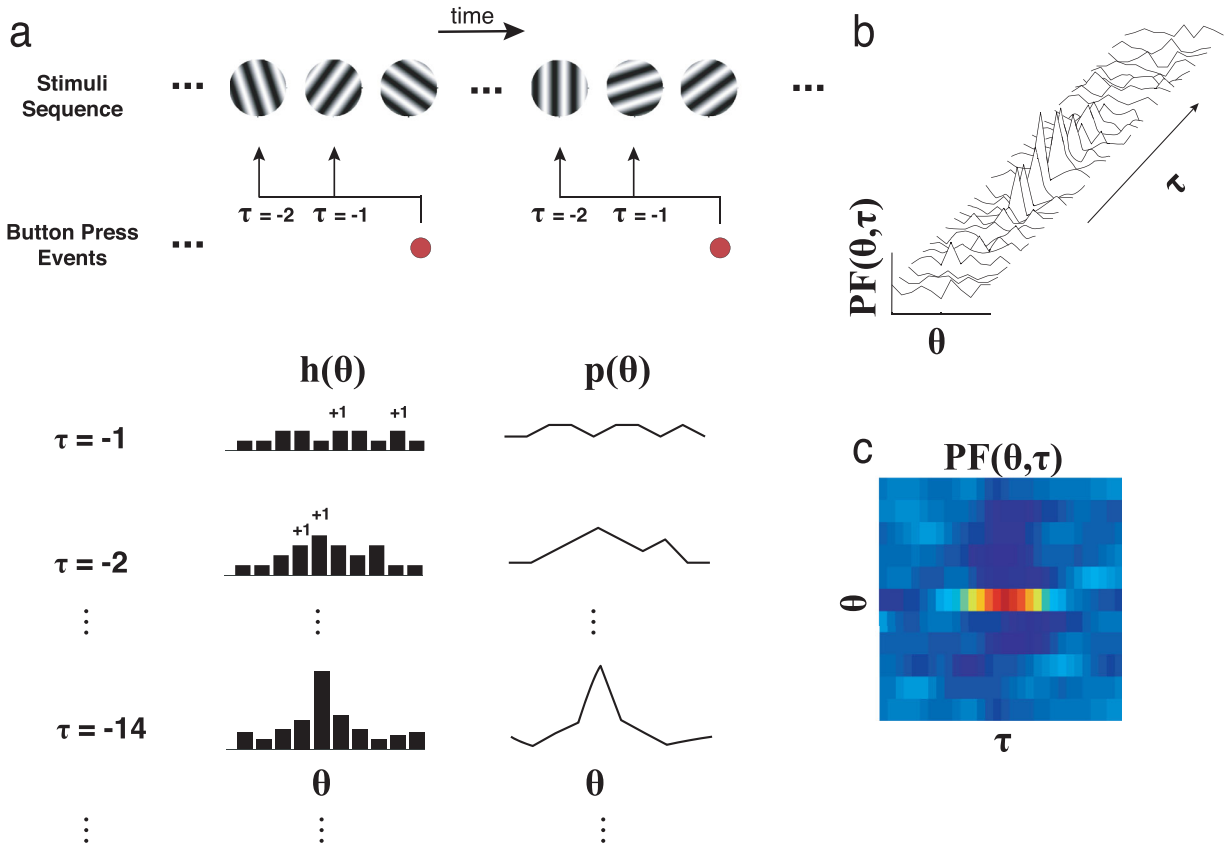

Figure 2. (**a**) An illustration of how the perceptive field is derived. The grating orientations within a 1 second period (30 gratings) prior to each response (key press) were piled together. The orientation histogram h(θ) was calculated for each time offset τ. The histogram was then divided by the total number of responses to get p(θ). The red circles represent timestamps of button presses. (**b**) The perceptive field PF(θ, τ) is the concatenation of p(θ) over all τs. (**c**) The perceptive field PF(θ, τ) as a heatmap.

$$\gamma(\tau) = 2\,\gamma_0 \phi\left(\frac{\tau-\tau_G}{\sigma_G}\right)\Phi\left(\eta_G\left(\frac{\tau-\tau_G}{\sigma_G}\right)\right), \qquad (3c)$$

where τ_E, τ_I, and τ_G determine the time corresponding to the peak, valley, and extremum of three components, respectively; σ_E, σ_I, and σ_G determine the widths of the distributions, respectively; η_E, η_I, and η_G determine the skewness of the distributions; a_0, β_0, and γ_0 are scaling factors that control the extrema of the components; $\varphi(\,)$ and $\Phi(\,)$ are the probability density and cumulative probability density functions of a standard normal distribution, respectively.

Equation 1 was fit to the smoothed PF(θ, τ) data by maximum likelihood procedure[63] to obtain the best fit parameters (κ_E, κ_I, τ_E, τ_I, τ_G, σ_E, σ_I, σ_G, η_E, η_I, η_G, a_0, β_0, γ_0, and c) and best fit PF(θ, τ) for each participant. The best-fitted PF was used in the comparison between the two groups. Because Equation 1 provided good fit to the data for all participants (χ^2 test, all $ps > 0.05$), we further calculated the r^2 of the model for each participant.

To compare the orientation-time PF between the two groups, a cluster-based permutation test,[64,65] was adopted. The test allowed us to look into the connected regions/areas in the orientation-time domain that differed between the amblyopic and normal groups. It has been proposed to deal with high dimensional data set in recent years, while keeping the family-wise error rate under control, and has been widely used in neuroscience for analyzing the electroencephalogram (EEG) or magnetoencephalography (MEG) data.[64,65]

After detecting particular regions in the orientation and time domains that differed significantly between PFs in the amblyopic and healthy groups, we then computed the orientation tuning curve and temporal response curve. The orientation tuning curve was calculated as the average PF(θ, τ) over time τ, weighted by its total squared deviation from uniformity at each τ:

$$\mathrm{OT}(\theta) = \frac{\sum_\tau w_\tau \mathrm{PF}(\theta,\tau)}{\sum_\tau w_\tau}, \qquad (4)$$

where, $w_\tau = \sum_\theta (\mathrm{PF}(\theta,\tau) - 0.1)^2$.

The temporal dynamics of PF was examined at two orientations, 90 degrees and 54 and 126 degrees (i.e. PF(90, τ) and PF(54/126, τ)). Specifically, we defined the temporal response curve:

$$\mathrm{PF}(90,\tau) = \alpha(\tau) + \beta(\tau) + \gamma(\tau) + c. \qquad (5)$$

Then *t*-tests were used to determine which parameters that differed in each domain, separately, serving as post hoc tests.

Results

We first looked at the response frequency (defined as the total number of key presses divided by the total number of the target, 5400) made by the amblyopic and healthy participants in the orientation identification task. There was no significant difference in response frequency between the amblyopic and control groups (0.086 ± 0.051 vs. 0.083 ± 0.041, $t(33) = 0.183$, $P = 0.856$).

The Perceptive Field

The best fit PFs are plotted as the upper and lower heatmaps, respectively, in each participant's panel of Figure 3. The time axis of the perceptive field is negative, relative to the time point of response. The model (Equation 1) provided a good fit to the PF for every participant (χ^2 test, all $ps > 0.05$). The fitting statistics of all participants were listed in Table A2, Appendix A. The PF of most participants showed similar characteristics: reaching maximum response at around -500 ms and becoming generally flat around −100 ms prior to the response. The responsive region had a peak at the target orientation (as expected), where it was excited by the stimuli, and two suppressive valleys at adjacent orientations, where the stimulus was less likely to drive responses. It is worthy to note that the PF of participants A1, A16, or A17 did not show any regularity like other participants with amblyopia (see Fig. 3). The coefficient of determination (r^2) of A1, A16, and A17 was significantly smaller than that of the rest of participants (0.329 ± 0.082 vs. 0.780 ± 0.088, $t(33) = 8.505$, $P < 0.001$; see Table A2, Appendix A). The data of A1, A16, and A17 were too noisy to reliably derive reasonable PF parameters. Thus, their results were excluded from the rest of the analyses. However, including these three participants will not change our results (Fig. A1, Appendix A).

To investigate the effect of amblyopia on the orientation tuning properties, the best-fit PF of the two groups were compared. The averaged (best fit) PF of the 14 amblyopic eyes (AE) and 18 dominant eyes (NE) of healthy participants are shown in Figures 4a and 4b, respectively, along with the difference between the two (Fig. 4c). As shown in the significance map (Fig. 4d), there were three regions where the PFs of the two groups differed. At the target orientation, from time -345 ms to -103 ms, the PF of the AE was significantly smaller than that of the NE ($P = 0.009$). At both orientations 54 degrees and 126 degrees, from time -310 ms to -241 ms,

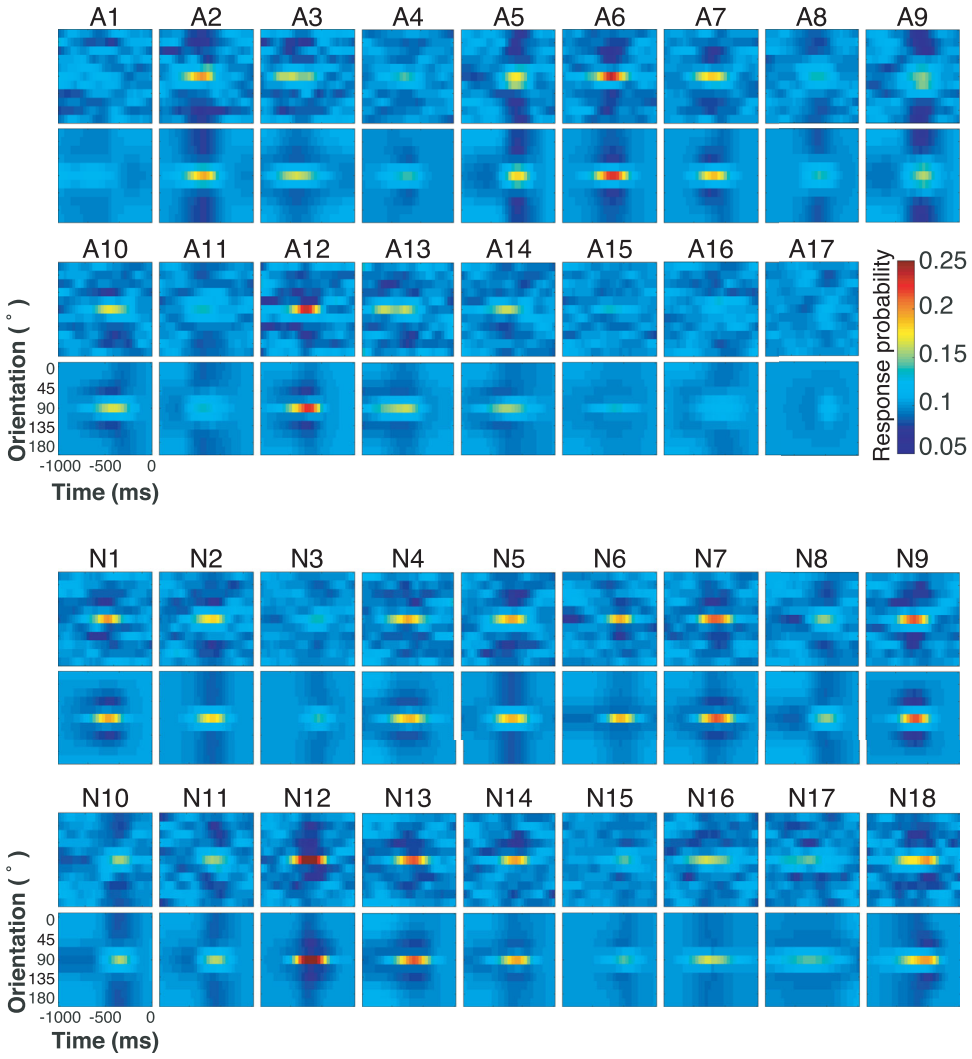

Figure 3. The smoothed (upper) and best fitted (lower) perceptive fields of the participants with amblyopia (approximately A1 to A17) and healthy participants (approximately N1 to N18). Difference in color indicates the response probability.

Investigative Ophthalmology & Visual Science

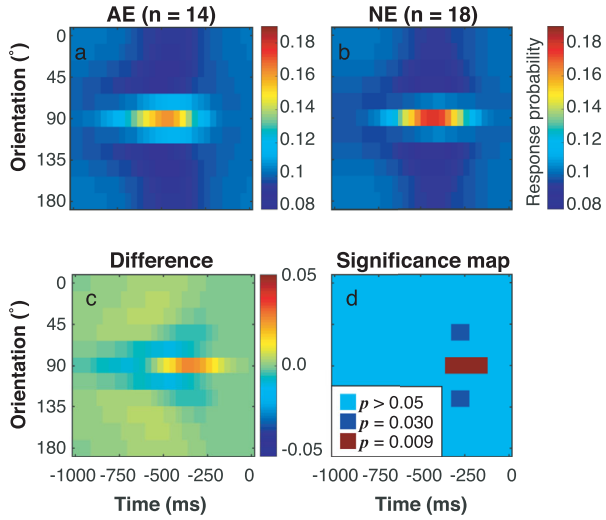

Figure 4. (**a**) The averaged perceptive field of the amblyopic group. (**b**) The averaged perceptive field of the control group. (**c**) The PF difference between the two groups **b** and **a**. The different color represents the value of response probability. (**d**) The statistical significance of each point of the PF difference based on the cluster-based permutation test. The color cyan indicates regions with $P > 0.05$. The red and blue colored areas indicate where the PFs in the two groups differ, but in different signs, respectively.

the response of the AE was significantly greater than that of the NE (both *p*s = 0.030). The result indicated that the PF of the AE differed from that of the NE in both orientation and time dimensions.

The Orientation Tuning

The orientation tuning curves of the two groups had a typical "Mexican hat" shape (Fig. 5a). To compare the shape of the orientation tuning between the two groups, the modulation depth of the response, defined by the difference between the maximum and minimum responses, and the full bandwidth at half difference between the maximum response and the response at orthogonal orientation of the orientation tuning curve were extracted (Fig. 5f). The bandwidth of the AE and NE were 31.41 ± 10.59 degrees and 24.76 ± 6.85 degrees, respectively. The AE had a larger bandwidth than that of the NE ($t(30) = 2.155$, $P = 0.039$; Fig. 5b). No difference in the modulation depth between two groups was found ($t(30) = 0.997$, $P = 0.327$; Fig. 5c). The correlation between the modulation depth and bandwidth was not significant ($r = -0.334$, $P = 0.243$). We also compared the width parameters κ_E and κ_I of the excitation and inhibition orientation tuning components (Equation 2) between the two groups. The width parameters κ_E ($t(30) = 2.581$, $P = 0.015$; Fig. 5d) and κ_I ($t(30) = 2.359$, $p = 0.025$, Fig. 5e) of the AE were smaller than those of the NE. The result indicated that the orientation tuning in the AE was broader than that in the NE (see Fig. 5).

The Temporal Dynamics

We then examined the dynamics of PF in temporal domain. In Figure 6a, the response at the target orientation (i.e. PF(90, τ) [temporal PF]), is plotted as a function of time for the two groups. The temporal PF of the AE and NE had a similar bell shape, increasing to the peak and then dropping down to the baseline before response. A one-dimensional cluster-based permutation test was used to compare the temporal dynamics of the PF between the two groups. The response of the AE was significantly lower than that of the NE from -310 ms to -103 ms (cluster-based permutation test, $P = 0.001$; see Fig. 6a). We also plotted the temporal curve at the most suppressive orientation (i.e. 54/126 degrees) in Figure 6b. The amblyopic eyes showed higher responses from -310 ms to -241 ms (cluster-based permutation test, $P = 0.006$). The shape parameters of the temporal PF, including the peak of target response (R_{peak}), the time corresponds to R_{peak} (reaction time [RT]), and the full width of half-height (FWHH) were also compared (Fig. 6g). The AE had a significantly longer RT than the NE (483 ms ± 68 ms vs. 425 ms ± 58 ms, $t(30) = 2.588$, $P = 0.015$; Fig. 6c). Neither R_{peak} ($t(30) = 1.283$, $P = 0.209$; Fig. 6d) nor FWHH ($t(30) = 0.183$, $P = 0.856$; Fig. 6e) showed any differences between the two groups. The peak time of the inhibition component (Equation 3b) τ_I of amblyopia was longer than that of the normal controls ($t(30) = 2.245$, $P = 0.032$; Fig. 6f). The results indicated that the main temporal change in the amblyopic PF was due to a general delay instead of the overall shape alternation.

Relationship Between Orientation Tuning and Contrast Sensitivity

To investigate how the PF changes in orientation-time domain related to the spatial vision in amblyopia, we performed correlation analyses. No significant correlation was found between the contrast sensitivity (CS) at spatial frequency (SF) of 1 c/deg (CS values of the amblyopic participants are listed in Table A1, Appendix A) and the bandwidth of the orientation tuning or RT in the amblyopic group (both *p*s > 0.05; Fig. 7).

Comparing PFs Between the Dominant and Non-Dominant Eyes

To rule out the possibility that the PF difference we found between the AE and NE was due to the choice of the dominant eye as the control eye, we additionally collected the PFs of the non-dominant eyes (NDE) from eight (of 18) normal participants, and compared the PFs between the dominant eye (DE) and NDE of these eight healthy participants. The PFs of the DE and NDE are shown in Figures 8a and 8b, respectively. The paired permutation test showed that there was no significant difference in any region of the PFs between DE and NDE of healthy participants ($P > 0.05$; Figs. 8c, 8d). Further analysis showed that there was no significant difference in either tuning bandwidth (24.7 ± 6.6 degrees vs. 25.6 ± 7.4 degrees, paired *t*-test, $t(7) = 0.585$, $P = 0.577$) or RT (418 ± 50 ms vs. 439 ± 59 ms, paired *t*-test, $t(7) = 0.905$, $P = 0.396$) between the DE and NDE.

Discussion

Summary

In this study, we asked participants to continuously detect vertical gratings embedded in a stream of randomly oriented gratings and estimated the orientation-time PF for the vertical grating detection task in the amblyopic and healthy

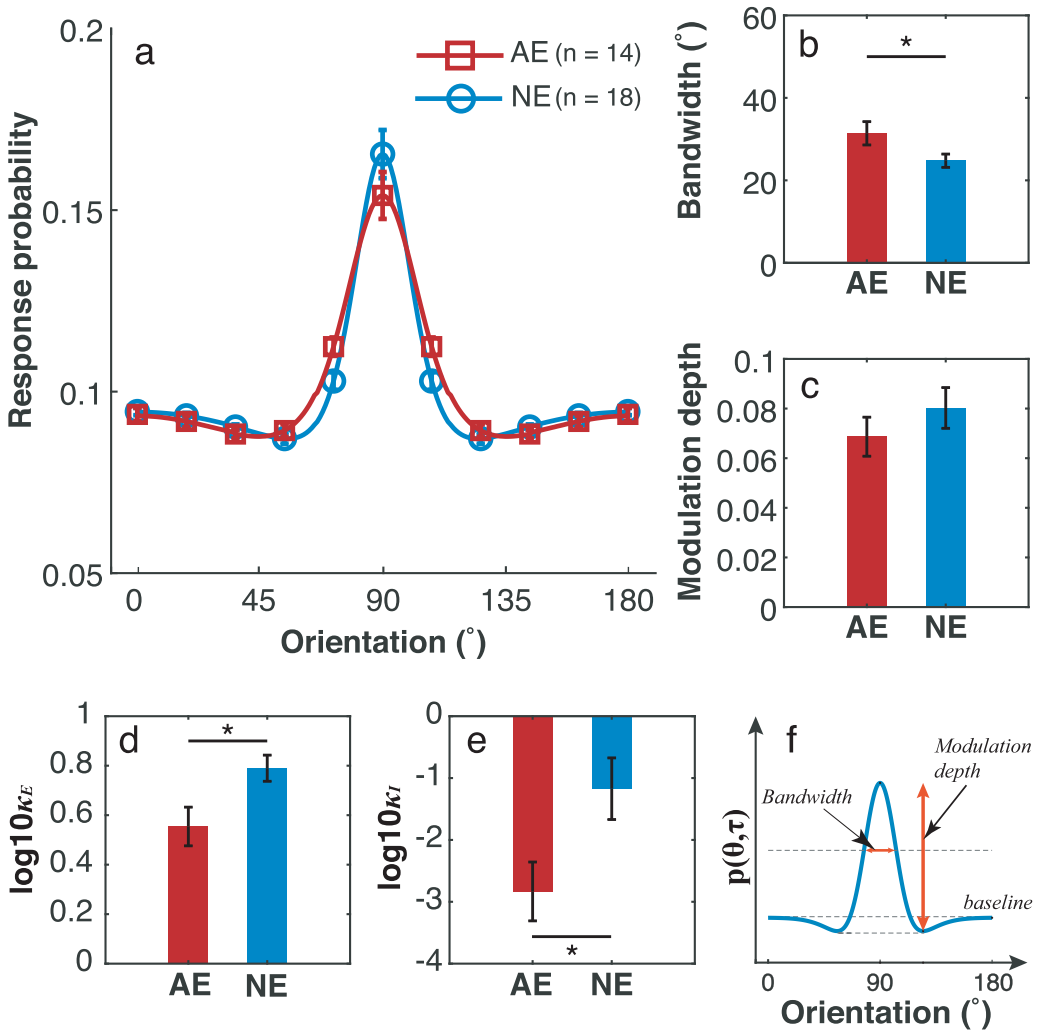

Figure 5. (**a**) The orientation tuning curves of the amblyopic (*red*) and the normal eye (*blue*). (**b**) The bandwidth of the participants with amblyopia was larger than that of the control participants. (**c**) No significant difference in the modulation depth was found. (**d**) Both κ_E and κ_I in the amblyopic group were significant smaller than that of the control group. Error bar: ±1 standard error. Asterisks: statistical significance with $P < 0.05$. (**f**) Shape analysis of the orientation tuning curve. The parameters used in the analysis are illustrated. The modulation depth of the response is defined by the difference between the maximum and minimum responses. The bandwidth is defined as full bandwidth at half difference between the maximum response and the response at its orthogonal orientation.

participants using a subspace reverse correlation technique.[26,48–50] Although no difference in the total response frequency was found between the amblyopic and control participants, the cluster-based permutation test revealed that there were significant differences in the PFs between the amblyopic and healthy eyes in both orientation and time domains. Further analyses showed that the orientation tuning curve in the AE was broader than that in the NE (see Fig. 5). The temporal dynamics of the PF in amblyopia showed a general delay (see Figs. 6a, 6b) instead of the shape change of response dynamics (see Fig. 6e). No difference in PFs between the DE and NDE in the normal group was found (see Fig. 8).

It has been reported that orientation discrimination sensitivity decreased with stimulus contrast.[66,67] Thus, we chose gratings of low spatial frequency and high contrast as our stimulus, aiming to equate the effective contrast of the stimulus in the amblyopic and healthy eyes. Although contrast sensitivity loss is the hallmark of amblyopia, the deficits are much more prominent at high spatial frequencies.[6,7,68] In addition, suprathreshold contrast perception of the amblyopic eyes was found to be largely normal.[69,70] To further confirm this, we additionally measured the CSFs of both DE and NDE of eight healthy participants, and compared these normal CSFs with those of the 12 amblyopic participants who had valid PF measures. The AE exhibited typical CSF deficits, with significantly reduced area under the CSF (AE vs. DE, $t(18) = 4.335$, $P < 0.001$; AE vs. NDE, $t(18) = 4.403$, $P < 0.001$; Fig. 9a). However, there was no sensitivity difference at 1 c/deg between the amblyopic and either of the healthy eyes (AE vs. DE, $t(18) = 1.290$, $P = 0.213$; AE vs. NDE, $t(18) = 1.167$, $P = 0.258$), as expected.

To rule out the possibility that the PF difference we found between the AE and NE was due to the eye dominance, we additionally collected the PFs of the non-dominant eyes from eight (of 18) healthy participants. No significant difference was found in any region of the PFs between the DE and NDE of the eight healthy participants (see Fig. 8). We further compared the bandwidth and RT between the AE and NDE. There was also no significant difference in

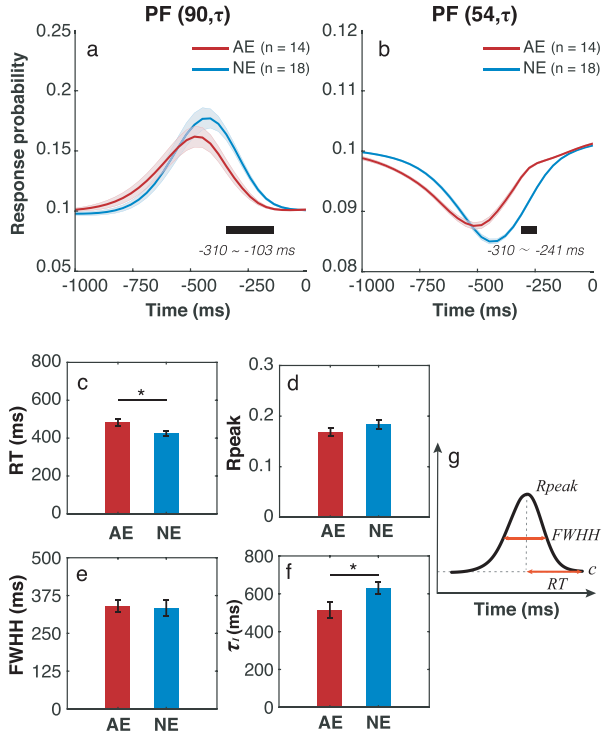

Figure 6. (**a**) The temporal dynamics of the perceptive field at the target orientation PF(90, τ). (**b**) The temporal dynamics of the perceptive field at the lateral orientation PF(54, τ). Note that PF(126, τ) is symmetrical to PF(54, τ). *Color red*: amblyopic eye; *color blue*: healthy eye. Transparent areas indicate ±1 standard error. The *thick black line* indicates the region where the two curves significantly differ. The comparisons of RT (**c**), R_{peak} (**d**), FWHH (**e**), and the peak time of the inhibition component (Equation 3b), τ_I (**f**) between the two groups. Error bar: ±1 standard deviation. Asterisks: statistical significance. (**g**) Shape analysis of the temporal response curve PF(90, τ). The peak of the PF at the target orientation (R_{peak}), the time corresponds to R_{peak} (RT), and the full width of half-height (FWHH) is illustrated.

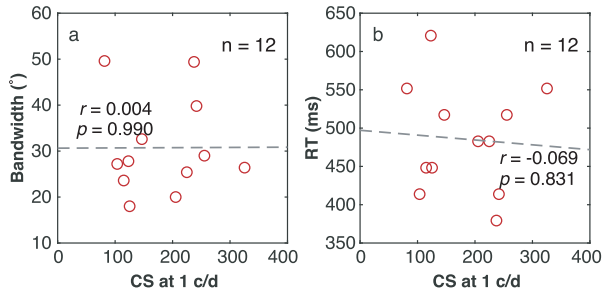

Figure 7. (**a**) The correlation between the bandwidth of the orientation tuning and the CS at 1 c/deg. (**b**) The correlation between the RT of the PF and the CS at 1 c/deg.

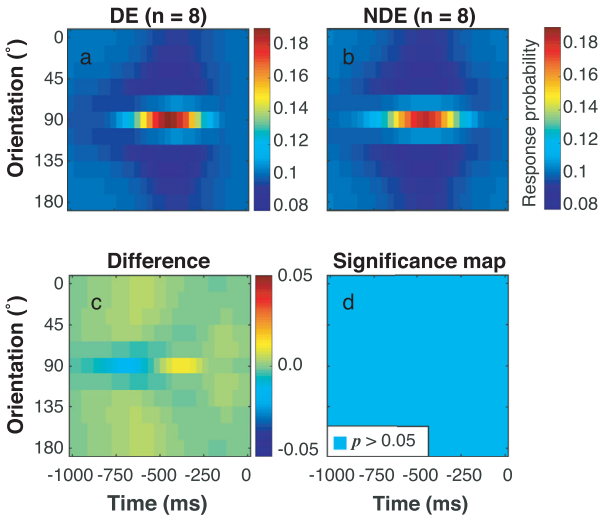

Figure 8. The average PFs of the DE (**a**) and NDE (**b**) of the eight healthy participants. (**c**) The PF difference of the DE and NDE, and (**d**) the corresponding significance map. The color cyan indicates regions with $P > 0.05$.

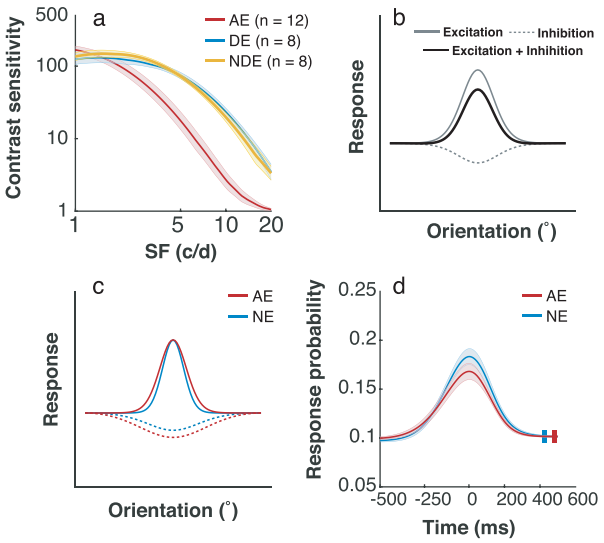

Figure 9. (**a**) The contrast sensitivity functions of the 12 amblyopic eyes (*red*), of the dominant eyes (DE, *blue*) of the eight normal participants, and of the non-dominant eyes (NDEs; *yellow*) of the same eight participants. (**b**) Illustrates the orientation tuning of a V1 neuron involves both the feedforward excitation from the lateral genius nucleus,[22] and the intra-cortical lateral inhibition.[26,34,35,71] (**c**) Both excitation and inhibition curves were broader in amblyopia. (**d**) The temporal response curve PF(90, τ) aligned to the peak. The short vertical bars denote the time participants responded. Shaded areas: ±1 standard error.

bandwidth ($t(20) = 1.360$, $P = 0.189$; Fig. 10a) or in RT ($t(20) = 1.511$, $P = 0.147$; Fig. 10b) between the AE and NDE. After inspection of the individual data of the bandwidth and RT (see Figs. 10a, 10b), we suspect that no statistical difference found between the AE and NDE was probably due to the insufficient sample size (8 NDEs). To overcome this, we used the bootstrap procedure to estimate the standard errors for bandwidth and RT of the AE ($n = 14$), DE ($n = 8$), and NDE ($n = 8$). There were 10,000 bootstrap samples of the bandwidth and RT that were generated for the AE, DE, and NDE, respectively, with the data for DE and NDE were always paired. Figure 10c shows that empirical distributions of the bandwidth samples for the AE, DE, and NDE. The Z test showed that the bandwidth difference between the AE and DE was significant ($z = 1.92$, $P = 0.028$). The bandwidth difference between the AE and NDE was marginally significant ($z = 1.602$, $P = 0.055$). There was no significant difference in bandwidth between the DE and NDE ($z = 0.611$, $P = 0.27$). Similar results for the RT samples can be seen in Figure 10d. There was a significant difference in RT between the AE

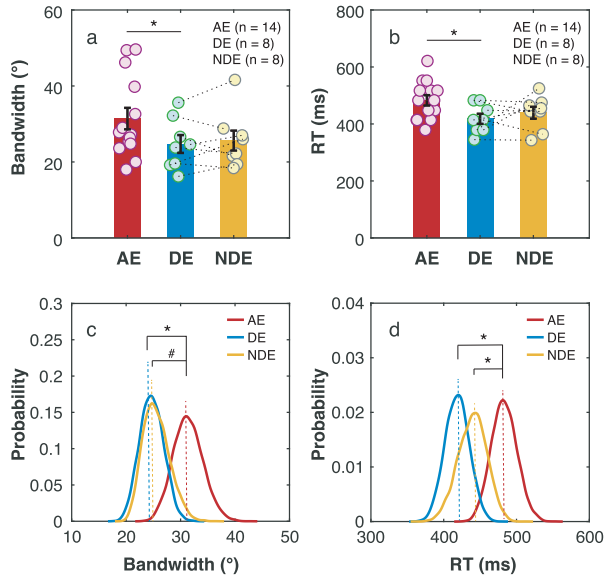

Figure 10. The tuning bandwidth (**a**) and RT of temporal dynamics (**b**) in the AE (*red*), DE (*blue*), and NDE (*yellow*). Each filled cycle denotes the data of each participant. The *black dotted lines* connect paired data of the DE and NDE. Error bar: ±1 standard deviation. The empirical distributions of the tuning bandwidth (**c**) and RT (**d**) were estimated from 10,000 bootstrap samples. The *dashed lines* indicate the means of the distributions. Asterisks: Statistical significance for $P < 0.05$. #: Marginal significance for $0.05 < P < 0.1$.

and DE ($z = 2.68$, $P = 0.004$), and between the AE and NDE ($z = 1.66$, $P = 0.048$). There was no significant difference in RT between the DE and NDE ($z = 0.956$, $P = 0.17$). Thus, the PF difference between the AE and DE we found in the study was not likely due to the choice of the dominant eye as the normal control group. Instead, it should be interpreted as reflecting the difference in orientation processing between the amblyopic and normal visual system.

The Orientation Tuning in Amblyopia

Psychophysical reverse correlation technique has been widely used to probe the early sensory processing in early visual cortex.[50,72,73] Especially with the task in which the participant was in control of the viewing duration, psychophysical reverse correlation offers the advantage of unbiased estimation of the sensory kernel.[51,74] By using the same paradigm of rapid presentation of gratings in different orientations, Roeber, Wong, and Freeman[48] showed that the paradigm could revoke strong cross-orientation suppression, which was tied with the sharpness of neural orientation tuning in visual cortex.[32,33] The PF estimated in our study is very similar to that found in the V1 neurons of awake macaques.[75] The orientation tuning curve we found had a typical "Mexican hat" shape, similar to that reported in V1 neurons[26] as well as in human observers.[50] In addition, the bandwidth of the healthy participants found in our experiment was also comparable with that measured in simple cells of macaque striate cortex[23] and in human observer.[76–78] Neurons at higher hierarchy of visual processing likely have larger receptive field[79] and broader tuning width.[80] As summarized by Cass, Stuit, Bex, and Alais,[78] the smallest bandwidth to the 1 c/deg grating reported in the literature was about 24 degrees, which is very close to what we found (26 degrees) here. Therefore, we believe that the orientation aspect of the estimated PF was more likely to reflect the tuning property of the low-level visual processing, and our result provided strong evidence for examining whether and how amblyopia affects orientation tuning in human.

We found that the orientation tuning in the amblyopic visual system was broader than that in the normal visual system. This is consistent to the result in a previous study, where Huang, Zhou, Liu, et al.[43] measured the monocular tilt illusion in patients with amblyopia, and suggested that the abnormal tilt illusion in amblyopia could be explained by a broader orientation tuning. Levi, Waugh, and Beard[47] also found that there were some of the amblyopic participants who showed broader orientation tuning. The shape and bandwidth of the orientation tuning estimated in our study are also within the range reported in the study by Levi, Waugh, and Beard.[47]

The width of excitation and inhibition tuning, reciprocally related to the parameters κ_E and κ_I, were found both wider in amblyopia (see Figs. 5d, 5e). The orientation tuning of a V1 neuron involves both the feedforward information from the lateral genius nucleus,[22] and the intra-cortical interaction[26,34,35] (see Fig. 9b). Our results might suggest that the geniculocortical feedforward input and intracortical lateral interactions in orientation processing are both affected in amblyopia (see Fig. 9c). There were human studies that demonstrated that the geniculocortical input and lateral interaction were impaired in amblyopia. Using high-resolution functional magnetic resonance imaging (fMRI), Wen, Wang, Zhou, et al.[81] found the amblyopic eye exhibited reduced response in the parvocellular layers of the lateral geniculate nucleus and weaker connection to V1. With psychophysical approaches, Polat, Sagi, and Norcia[82] and Polat, Ma-Naim, Belkin, and Sagi[83] reported that the abnormal spatial interaction in patients with amblyopia suggested the horizontal connections in primary visual cortex were disrupted.

The Response Dynamics in Amblyopia

Psychophysical reverse correlation could also provide the temporal dynamics of the visual processing. The PF was essentially the histogram of stimulus orientations of all responses at different time (see Fig. 2). The temporal spread of the PF essentially reflected the variability of the RT across trials. There was no difference in FWHH of the temporal response curve, PF(90, τ), between the two groups. When we aligned the peak time of the temporal PFs of the two groups, it is evident that the shape of the temporal PF of the two groups was similar (see Fig. 9d). The result suggests that the RT variability of the AE and NE was comparable.

The orientation-time PF is information-rich, as it encompasses the entire temporal course from the neural processing delay from the retina to the brain and from the brain to the muscles. The RT of the temporal response curve was more than 400 ms, which is much greater than that of neural responses in V1.[26,71,84] Thus, the RT possibly contained a substantial component taken by the processing at downstream visual areas of V1. The AE showed a significantly longer RT than the NE(DE), which is consistent with previous works involving psychophysics[85–87] or EEG measurement.[88] The temporal response curve had a flat region that followed the hump, where the stimulus had no influence on the response (see Fig. 6a, Fig. 9d). This region set the lower limit of the RT which is believed to consist of the

time needed to generate the internal representation from the stimulus, and the post-sensory delay that is needed to execute the response.[51,89,90] Given that the FWHHs of the temporal response curve in the AE and NE were similar, and that the effective contrast between the AE and NE were equated, we thus speculated that the prolonged RT in amblyopia possibly reflected the post-sensory delay at downstream visual areas of V1. Similar to our finding, Farzin and Norcia[87] has also reported that the prolonged RT in amblyopia was independent of visual acuity and suggested the cortical connections to higher brain areas underlying decision and response selection processes were affected by amblyopia.

Conclusion

In conclusion, using a subspace reverse correlation paradigm with gratings of 1 c/deg and 99% contrast, we found an altered orientation-time PF in amblyopia characterized by a broader tuning width and general temporal delay. Our result suggests that amblyopia may lead to abnormal feedforward geniculocortical input and lateral intracortical connections, and higher level deficit that related to downstream processing. Our study sheds light on the mechanisms underlying the deficits of orientation processing in amblyopia. It also bridges the gap between the findings at single cell and behavioral levels and provides rigorous constraint for models of orientation selectivity.

Acknowledgments

The authors thank Peng Zhang for helping us with the cluster-based permutation test. We are also grateful to the anonymous reviewers for their constructive suggestions.

Supported by National Key Research and Development Program of China (2020YFC2003800 to C.B.H.), the National Natural Science Foundation of China (NSFC81600764 to F.H.; NSFC 32071056 and 32100864 to C.B.H.), the Department of Human Resources and Social Security of Zhejiang Province (Qianjiang Talent Project, QJD1803028 to F.H.), Wenzhou Science and Technology Bureau (Y20180710 to X.R.), the Scientific Instrument Developing Project of the Chinese Academy of Sciences (ZDKYYQ20200005 to C.B.H.).

Disclosure: **J. Zhu**, None; **X. Ruan**, None; **C. Li**, None; **J. Yuan**, None; **Y. Yang**, None; **W. Zhang**, None; **H. Zhang**, None; **Z. Zhuo**, None; **F.-F. Yan**, None; **C.-B. Huang**, None; **F. Hou**, None

References

1. Birch EE. Amblyopia and binocular vision. *Prog Retin Eye Res*. 2013;33:67–84.
2. DeSantis D. Amblyopia. *Pediatr Clin North Am*. 2014;61:505–518.
3. Friendly DS. Amblyopia: definition, classification, diagnosis, and management considerations for pediatricians, family physicians, and general practitioners. *Pediatr Clin North Am*. 1987;34:1389–1401.
4. McKee SP, Levi DM, Movshon JA. The pattern of visual deficits in amblyopia. *J Vis*. 2003;3:380–405.
5. Ciuffreda KJ, Levi DM, Selenow A. *Amblyopia: Basic and Clinical Aspects*. Oxford, England: Butterworth-Heinemann; 1991.
6. Bradley A, Freeman RD. Contrast sensitivity in anisometropic amblyopia. *Invest Ophthalmol Vis Sci*. 1981; 21:467–476.
7. Hess RF, Howell ER. The threshold contrast sensitivity function in strabismic amblyopia: evidence for a two type classification. *Vis Res*. 1977;17:1049–1055.
8. Hilz R, Rentschler I, Brettel H. Myopic and strabismic amblyopia: substantial differences in human visual development. *Exp Brain Res*. 1977;30:445–446.
9. Selby SA, Woodhouse JM. The spatial frequency dependence of interocular transfer in amblyopes. *Vis Res*. 1981;21:1401–1408.
10. Hou F, Huang C-B, Lesmes L, et al. qCSF in Clinical Application: Efficient Characterization and Classification of Contrast Sensitivity Functions in Amblyopia. *Invest Opthalmol Vis Sci*. 2010;51:5365–5377.
11. Walraven J, Janzen P. TNO stereopsis test as an aid to the prevention of amblyopia. *Ophthalmic Physiol Opt*. 1993;13:350–356.
12. Huang CB, Zhou J, Lu ZL, Feng L, Zhou Y. Binocular combination in anisometropic amblyopia. *J Vis*. 2009;9(17):11–16.
13. Kozma P, Kiorpes L. Contour integration in amblyopic monkeys. *Vis Neurosci*. 2003;20:577–588.
14. Kovacs I, Polat U, Pennefather PM, Chandna A, Norcia AM. A new test of contour integration deficits in patients with a history of disrupted binocular experience during visual development. *Vis Res*. 2000;40:1775–1783.
15. Wu C, Hunter DG. Amblyopia: diagnostic and therapeutic options. *Am J Ophthalmol*. 2006;141:175–184.
16. Duffy FH, Burchfiel JL, Snodgrass SR. The pharmacology of amblyopia. *Ophthalmology*. 1978;85:489–495.
17. Hess RF. Is amblyopia an impediment to binocular function? *Eye (Lond)*. 1996;10 (Pt 2):245–249.
18. Epelbaum M, Milleret C, Buisseret P, Dufier JL. The sensitive period for strabismic amblyopia in humans. *Ophthalmology*. 1993;100:323–327.
19. Wiesel TN, Hubel DH. Effects of Visual Deprivation on Morphology and Physiology of Cells in the Cats Lateral Geniculate Body. *J Neurophysiol*. 1963;26:978–993.
20. Hubel DH, Wiesel TN. The period of susceptibility to the physiological effects of unilateral eye closure in kittens. *J Physiol*. 1970;206:419–436.
21. Priebe NJ. Mechanisms of Orientation Selectivity in the Primary Visual Cortex. *Ann Rev Vis Sci*. 2016;2:85–107.
22. Hubel DH, Wiesel TN. Receptive fields, binocular interaction and functional architecture in the cat's visual cortex. *J Physiol*. 1962;160:106–154.
23. De Valois RL, Yund EW, Hepler N. The orientation and direction selectivity of cells in macaque visual cortex. *Vis Res*. 1982;22:531–544.
24. Ferster D, Miller KD. Neural mechanisms of orientation selectivity in the visual cortex. *Ann Rev Neurosci*. 2000;23:441–471.
25. Vanduffel W, Tootell RBH, Schoups AA, Orban GA. The Organization of Orientation Selectivity Throughout Macaque Visual Cortex. *Cerebral Cortex*. 2002;12:647–662.
26. Ringach DL, Hawken MJ, Shapley R. Dynamics of orientation tuning in macaque V1: the role of global and tuned suppression. *J Neurophysiol*. 2003;90:342–352.
27. Somers DC, Nelson SB, Sur M. An emergent model of orientation selectivity in cat visual cortical simple cells. *J Neurosci*. 1995;15:5448–5465.
28. Douglas RJ, Koch C, Mahowald M, Martin KA, Suarez HH. Recurrent excitation in neocortical circuits. *Science*. 1995;269:981–985.
29. Gardner JL, Anzai A, Ohzawa I, Freeman RD. Linear and nonlinear contributions to orientation tuning of simple cells in the cat's striate cortex. *Vis Neurosci*. 1999;16:1115–1121.
30. Sclar G, Freeman RD. Orientation selectivity in the cat's striate cortex is invariant with stimulus contrast. *Exp Brain Res*. 1982;46:457–461.

31. Skottun BC, Bradley A, Sclar G, Ohzawa I, Freeman RD. The effects of contrast on visual orientation and spatial frequency discrimination: a comparison of single cells and behavior. *J Neurophysiol*. 1987;57:773–786.
32. Nauhaus I, Benucci A, Carandini M, Ringach DL. Neuronal selectivity and local map structure in visual cortex. *Neuron*. 2008;57:673–679.
33. Koch E, Jin J, Alonso JM, Zaidi Q. Functional implications of orientation maps in primary visual cortex. *Nat Commun*. 2016;7:13529.
34. Moore BDt, Freeman RD. Development of orientation tuning in simple cells of primary visual cortex. *J Neurophysiol*. 2012;107:2506–2516.
35. Malach R, Amir Y, Harel M, Grinvald A. Relationship between intrinsic connections and functional architecture revealed by optical imaging and in vivo targeted biocytin injections in primate striate cortex. *Proc Natl Acad Sci USA*. 1993;90:10469–10473.
36. Chino YM, Smith EL, 3rd, Wada H, Ridder WH, 3rd, Langston AL, Lesher GA. Disruption of binocularly correlated signals alters the postnatal development of spatial properties in cat striate cortical neurons. *J Neurophysiol*. 1991;65:841–859.
37. Crewther DP, Crewther SG. Neural site of strabismic amblyopia in cats: spatial frequency deficit in primary cortical neurons. *Exp Brain Res*. 1990;79:615–622.
38. Stryker MP, Sherk H. Modification of cortical orientation selectivity in the cat by restricted visual experience: a reexamination. *Science*. 1975;190:904–906.
39. Kiorpes L, Kiper DC, O'Keefe LP, Cavanaugh JR, Movshon JA. Neuronal Correlates of Amblyopia in the Visual Cortex of Macaque Monkeys with Experimental Strabismus and Anisometropia. *J Neurosci*. 1998;18:6411–6424.
40. Bi H, Zhang B, Tao X, Harwerth RS, Smith EL, 3rd, Chino YM. Neuronal responses in visual area V2 (V2) of macaque monkeys with strabismic amblyopia. *Cerebral Cortex (New York, NY: 1991)*. 2011;21:2033–2045.
41. Skottun BC, Bradley A, Freeman RD. Orientation discrimination in amblyopia. *Invest Ophthalmol Vis Sci*. 1986;27:532–537.
42. John R. Contrast Detection and Orientation Discrimination Thresholds Associated with Meridional Amblyopia. *Vis Res*. 1997;37:1451–1457.
43. Huang J, Zhou Y, Liu C, Liu Z, Luan C, Tzvetanov T. The neural basis of spatial vision losses in the dysfunctional visual system. *Sci Rep*. 2017;7:11376.
44. Demanins R, Hess RF, Williams CB, Keeble DR. The orientation discrimination deficit in strabismic amblyopia depends upon stimulus bandwidth. *Vis Res*. 1999;39:4018–4031.
45. Kiorpes L. Visual processing in amblyopia: animal studies. *Strabismus*. 2006;14:3–10.
46. Kiorpes L. Understanding the development of amblyopia using macaque monkey models. *Proc Natl Acad Sci*. 2019;116:26217–26223.
47. Levi DM, Waugh SJ, Beard BL. Spatial scale shifts in amblyopia. *Vis Res*. 1994;34:3315–3333.
48. Roeber U, Wong EMY, Freeman AW. Cross-orientation interactions in human vision. *J Vis*. 2008;8:1–11.
49. Ringach D, Shapley R. Reverse correlation in neurophysiology. *Cogn Sci*. 2004;28:147–166.
50. Ringach DL. Tuning of orientation detectors in human vision. *Vis Res*. 1998;38:963–972.
51. Okazawa G, Sha L, Purcell BA, Kiani R. Psychophysical reverse correlation reflects both sensory and decision-making processes. *Nature Communications*. 2018;9:3479.
52. Neri P, Levi DM. Receptive versus perceptive fields from the reverse-correlation viewpoint. *Vis Res*. 2006;46:2465–2474.
53. Murray RF. Classification images: A review. *J Vis*. 2011;11:2–2.
54. Zheng H, Shen M, He X, et al. Comparing Spatial Contrast Sensitivity Functions Measured With Digit and Grating Stimuli. *Transl Vis Sci Technol*. 2019;8:16.
55. Ho R, Thompson B, Babu RJ, Dalton K. Sighting ocular dominance magnitude varies with test distance. *Clin Exp Optom*. 2018;101:276–280.
56. Kleiner M, Brainard D, Pelli D. What's new in Psychtoolbox-3?. *Perception*. 2007;36:1–16.
57. Hallum LE, Cloherty SL. Liquid-Crystal Display (LCD) of achromatic, mean-modulated flicker in clinical assessment and experimental studies of visual systems. *PLoS One*. 2021;16:e0248180.
58. Elze T, Tanner TG. Temporal properties of liquid crystal displays: implications for vision science experiments. *PLoS One*. 2012;7:e44048.
59. Li X, Lu ZL. Enabling high grayscale resolution displays and accurate response time measurements on conventional computers. *J Vis Exp*. 2012;60:3312.
60. Moore MD, McGarvey MJ, Russell RA, Cullen BR, McClure MO. Stable inhibition of hepatitis B virus proteins by small interfering RNA expressed from viral vectors. *J Gene Med*. 2005;7:918–925.
61. Mardia K. *Statistics of Directional Data*. London, UK: Academic;1972.
62. Pewsey A. Problems of inference for Azzalini's skew normal distribution. *J Appl Stat*. 2000;27: 859–870.
63. Watson AB. Probability summation over time. *Vis Res*. 1979;19:515–522.
64. Maris E, Oostenveld R. Nonparametric statistical testing of EEG- and MEG-data. *J Neurosci Methods*. 2007;164:177–190.
65. Pernet CR, Latinus M, Nichols TE, Rousselet GA. Cluster-based computational methods for mass univariate analyses of event-related brain potentials/fields: A simulation study. *J Neurosci Methods*. 2015;250:85–93.
66. Webster MA, De Valois KK, Switkes E. Orientation and spatial-frequency discrimination for luminance and chromatic gratings. *J Opt Soc Am A*. 1990;7:1034–1049.
67. DiMattina C. Comparing models of contrast gain using psychophysical experiments. *J Vis*. 2016;16:1-1.
68. Volkers AC, Hagemans KH, van der Wildt GJ, Schmitz PI. Spatial contrast sensitivity and the diagnosis of amblyopia. *Br J Ophthalmol*. 1987;71:58–65.
69. Hess RF, Bradley A, Piotrowski L. Contrast-coding in amblyopia. I. Differences in the neural basis of human amblyopia. *Proc R Soc Lond B Biol Sci*. 1983;217:309–330.
70. Loshin DS, Levi DM. Suprathreshold contrast perception in functional amblyopia. *Documenta Ophthalmologica Advances in Ophthalmol*. 1983;55:213–236.
71. Ringach DL, Hawken MJ, Shapley R. Dynamics of orientation tuning in macaque primary visual cortex. *Nature*. 1997;387:281–284.
72. Ahumada AJ, Jr. Classification image weights and internal noise level estimation. *J Vis*. 2002;2:8.
73. Knoblauch K, Maloney LT. Estimating classification images with generalized linear and additive models. *J Vis*. 2008;8:10.
74. Stine GM, Zylberberg A, Ditterich J, Shadlen MN. Differentiating between integration and non-integration strategies in perceptual decision making. *Elife*. 2020;9:e55365.
75. Mazer JA, Vinje WE, McDermott J, Schiller PH, Gallant JL. Spatial frequency and orientation tuning dynamics in area V1. *Proc Natl Acad Sci*. 2002;99:1645–1650.
76. Campbell FW, Kulikowski JJ. Orientational selectivity of the human visual system. *J Physiol*. 1966;187:437–445.

Investigative Ophthalmology & Visual Science

77. Thomas JP, Gille J. Bandwidths of orientation channels in human vision. *J Opt Soc Am*. 1979;69:652–660.
78. Cass J, Stuit S, Bex P, Alais D. Orientation bandwidths are invariant across spatiotemporal frequency after isotropic components are removed. *J Vis*. 2009;9:17.
79. Smith AT, Singh KD, Williams AL, Greenlee MW. Estimating Receptive Field Size from fMRI Data in Human Striate and Extrastriate Visual Cortex. *Cerebral Cortex*. 2001;11:1182–1190.
80. David SV, Hayden BY, Gallant JL. Spectral Receptive Field Properties Explain Shape Selectivity in Area V4. *J Neurophysiol*. 2006;96:3492–3505.
81. Wen W, Wang Y, Zhou J, et al. Loss and enhancement of layer-selective signals in geniculostriate and corticotectal pathways of adult human amblyopia. *Cell Rep*. 2021;37:110117.
82. Polat U, Sagi D, Norcia AM. Abnormal long-range spatial interactions in amblyopia. *Vis Res*. 1997;37:737–744.
83. Polat U, Ma-Naim T, Belkin M, Sagi D. Improving vision in adult amblyopia by perceptual learning. *Proc Natl Acad Sci USA*. 2004;101:6692–6697.
84. Gillespie DC, Lampl I, Anderson JS, Ferster D. Dynamics of the orientation-tuned membrane potential response in cat primary visual cortex. *Nature Neurosci*. 2001;4:1014–1019.
85. Hamasaki DI, Flynn JT. Amblyopic eyes have longer reaction times. *Invest Ophthalmol Vis Sci*. 1981;21:846–853.
86. Chino YM, Shansky MS, Jankowski WL, Banser FA. Effects of rearing kittens with convergent strabismus on development of receptive-field properties in striate cortex neurons. *J Neurophysiol*. 1983;50:265–286.
87. Farzin F, Norcia AM. Impaired visual decision-making in individuals with amblyopia. *J Vis*. 2011;11:10.1167.
88. Wang J, Zhao J, Wang S, Gong R, Zheng Z, Liu L. Cognitive processing of orientation discrimination in anisometropic amblyopia. *PLoS One*. 2017;12:e0186221.
89. Weindel G, Gajdos T, Burle B, Alario F-X. The Decisive Role of Non-Decision Time for Interpreting the Parameters of Decision Making Models. *Neuropsychologia* 2020;146:107560.
90. Ratcliff R, McKoon G. The diffusion decision model: theory and data for two-choice decision tasks. *Neural Computation*. 2008;20:873–922.

Investigative Ophthalmology & Visual Science

Appendix A

The detailed information of the amblyopic participants is listed in Table A1. The goodness of fit of Equation 1, including χ^2 statistics and r^2, for each participant is listed in Table A2. When all participants were included, the cluster-based permutation test showed that the differences between the AE and NE were significant (Fig. A1).

Table A1. Characteristics of the Amblyopic[a] Participants

No.	Sex	Age	Eye	Type[b]	Correction	VA[c]	CS[d] at 1 c/deg	Experienced
1	F	32	NAE	Aniso	+0.25DS/−0.50DC × 130	−0.1	N/A	Yes
			AE		+5.00DS/−1.00DC × 15	0.5	53	
2	F	28	AE	Depri	−2.25DS	0.4	N/A	Yes
			AE		−3.00DS	0.7	147	
3	M	22	NAE	Aniso	−4.00DS	−0.1	N/A	Yes
			AE		+5.00DS	0.6	123	
4	M	45	AE	Aniso	+7.75DS	0.2	N/A	Yes
			AE		+6.50DS	0.1	255	
5	M	36	AE	Aniso	+5.50DS/+1.0DC × 170	0.8	242	Yes
			NAE		−2.75DS	0.0	N/A	
6	M	27	NAE	Aniso	−4.75DS/−1.25DC × 18	−0.1	N/A	Yes
			AE		+0.25DS	0.3	115	
7	M	22	NAE	Aniso	−4.75DS	0.2	N/A	Yes
			AE		+3.00DS	0.5	225	
8	F	38	NAE	Mixed	−2.75DS/−0.50DC × 30	0.0	N/A	No
			AE		+2.25DS/−0.50DC × 150	0.3	N/A	
9	M	21	NAE	Aniso	−0.75DS	0.0	N/A	No
			AE		+0.50DS/−0.50DC × 180	0.3	237	
10	F	20	NAE	Aniso	−1.50DS	0.05	N/A	No
			AE		+6.00DS/−1.00DC × 170	0.5	104	
11	M	25	AE	Aniso	−14.75DS/−1.0DC × 180	0.7	82	Yes
			NAE		−7.75DS/−0.75DC × 10	0.0	N/A	
12	F	27	NAE	Aniso	Plano	−0.1	N/A	Yes
			AE		+1.0DS/−0.50DS × 180	0.4	205	
13	F	25	NAE	Aniso	−0.50DS	0.0	N/A	Yes
			AE		+4.50DS/−0.75DC × 15	0.5	325	
14	F	22	NAE	Aniso	−0.50DS	0.0	N/A	Yes
			AE		+2.75DS/−0.50DC × 180	0.1	N/A	
15	F	26	NAE	Mixed	−3.75DS/−0.50DC × 80	0.0	N/A	No
			AE		+1.25DS	0.1	125	
16	M	26	AE	Aniso	+4.50DS/−0.50DC × 170	0.8	165	No
			NAE		−0.50DS/−0.25DC × 30	−0.1	N/A	
17	F	18	NAE	Aniso	−2.75.50DS/−1.00DC × 5	0.0	N/A	No
			AE		+0.25DS/−1.50DC × 175	0.1	130	

[a] A14, A15 and A17 are "treated" amblyopes. The PFs of A14, A15 and A17 were more similar to those of amblyopic group than the normal group. After excluding these three "treated amblyopes," our result still held.

[b] Mixed types of amblyopia with strabismus and anisometropia. Participant A8 used to be esotropia and her eye position been surgically corrected. Her original eye position was not available. Participant A15 used to be intermittent exotropia and the eye position has been surgically corrected. Her original eye position was −18Δ at distance and −8Δ at near. At the time of experiment, both A8 and A15 have correct eye alignment.

[c] Acuity is expressed in Logarithm of the Minimum Angle of Resolution (logMAR).

[d] CS at 1 c/deg was 138 ± 25 (mean ± SD) for the dominant eye of the 8 healthy participants, and 145 ± 21 for the non-dominant eye of the same eight normal participants, respectively. There was no sensitivity difference at 1 c/deg between the amblyopic and either of the normal eyes (AE vs. DE, $t(18) = 1.290$, $P = 0.213$; AE vs. NDE, $t(18) = 1.167$, $P = 0.258$).

AE, amblyopic eye; Aniso, anisometropia; CS, contrast sensitivity; NAE, non-amblyopia eye; VA, visual acuity.

Investigative Ophthalmology & Visual Science

Table A2. Goodness of Fit of the Model for All Participants

Participant		χ^2	p	r^2
Amblyopia	A1	2985.1	1	0.300
	A2	2384.2	1	0.796
	A3	1507.3	1	0.677
	A4	5984.6	1	0.670
	A5	5900.1	1	0.857
	A6	3978.7	1	0.899
	A7	4257.6	1	0.836
	A8	10361.3	1	0.790
	A9	5957.1	1	0.835
	A10	5027.3	1	0.792
	A11	5121.1	1	0.708
	A12	2170.6	1	0.734
	A13	2479.2	1	0.671
	A14	4788.1	1	0.769
	A15	6239.5	1	0.528
	A16	3736.6	1	0.421
	A17	14,071.3	1	0.265
Normal	N1	4251.1	1	0.815
	N2	3757.0	1	0.757
	N3	9432.3	1	0.664
	N4	3300.0	1	0.794
	N5	5342.5	1	0.840
	N6	4506.6	1	0.785
	N7	5584.2	1	0.902
	N8	10,331.4	1	0.825
	N9	2850.0	1	0.848
	N10	8172.3	1	0.842
	N11	6805.4	1	0.669
	N12	2098.2	1	0.934
	N13	3634.6	1	0.895
	N14	3665.2	1	0.804
	N15	6546.0	1	0.770
	N16	3525.3	1	0.704
	N17	3172.0	1	0.704
	N18	2281.6	1	0.834

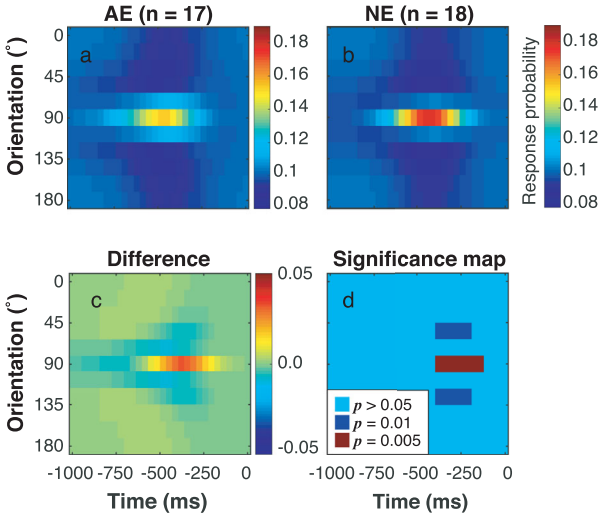

Figure A1. (**a**) The averaged perceptive field of all 17 amblyopic participants. (**b**) The averaged perceptive field of the control group. (**c**) The PF difference between the two groups **b** and **a**. Different color represents the value of response probability. (**d**) The statistical significance of each point of the PF difference based on the cluster-based permutation test. The color cyan indicates regions with $P > 0.05$. The red and blue colors indicate where the PFs in the two groups differ, but in different signs, respectively.